J Seismol (2017) 21:825–836
DOI 10.1007/s10950-016-9637-x

ORIGINAL ARTICLE

Mantle upwelling beneath Madagascar: evidence from receiver function analysis and shear wave splitting

Jonathan D. Paul · Caroline M. Eakin

Received: 22 October 2015 / Accepted: 21 December 2016 / Published online: 9 January 2017

Abstract Crustal receiver functions have been calculated from 128 events for two three-component broadband seismomenters located on the south coast (FOMA) and in the central High Plateaux (ABPO) of Madagascar. For each station, crustal thickness and V_p/V_s ratio were estimated from H-κ plots. Self-consistent receiver functions from a smaller back-azimuthal range were then selected, stacked and inverted to determine shear wave velocity structure as a function of depth. These results were corroborated by guided forward modeling and by Monte Carlo error analysis. The crust is found to be thinner (39 ± 0.7 km) beneath the highland center of Madagascar compared to the coast (44 ± 1.6 km), which is the opposite of what would be expected for crustal isostasy, suggesting that present-day long wavelength topography is maintained, at least in part, dynamically. This inference of dynamic support is corroborated by shear wave splitting analyses at the same stations, which produce an overwhelming majority of null results (>96 %), as expected for vertical mantle flow or asthenospheric upwelling beneath the island. These findings suggest a sub-plate origin for dynamic support.

Keywords Receiver function · Madagascar · Crustal structure · Moho discontinuity · Dynamic support

J. D. Paul (✉)
Bullard Laboratories, Department of Earth Sciences, University of Cambridge, Madingley Road, Cambridge, CB3 0EZ, UK
e-mail: jdp@cantab.net

J. D. Paul
Department of Earth Sciences, University College London, Gower St., London, WC1E 6BT, UK

C. M. Eakin
Ocean and Earth Science, University of Southampton, National Oceanography Centre Southampton, Southampton, SO14 3ZH, UK

C. M. Eakin
Research School of Earth Sciences, Australian National University, 142 Mills Road, Acton ACT, 2601 Australia

1 Introduction

The youthful nature of Madagascar's landscape contrasts against the Pan-African-aged basement schists and gneisses, which comprise the majority of the island's bedrock geology (De Wit 2003). Heavily weathered and dissected peneplains form the surface expression of rapid erosion rates, amongst the highest in the world and not solely resulting from human activities such as deforestation and slash-and-burn farming practices (Bourgeat and Petit 1969; Wells and Andriamihaja 1993; Kusky et al. 2010). Roberts et al. (2012) inverted longitudinal river profiles to argue for rapid (0.2–0.3 km Myr^{-1}) surface uplift during Neogene times.

Madagascar's location and a +30 mGal long wavelength free-air gravity anomaly centered on the island suggest its topography is maintained dynamically at long (∼1000 km) wavelengths (Fig. 1; Al-Hajri et al. 2010; Roberts et al. 2012). Three sets of observations suggest that this phenomenon could reflect a mantle upwelling. First, the gravity anomaly is similar in amplitude and wavelength to anomalies associated with topographic domes in West Africa (e.g. Bié, Namibia), which have 0.5–1 km of dynamic support (Al-Hajri et al. 2010). Secondly, there is excellent evidence for a large, seismically slow region beneath southern Africa and its surroundings (e.g. Panning and Romanowicz 2006; Simmons et al. 2009); Madagascar is on the edge of a large, slow velocity anomaly. It is generally agreed that slow seismic velocities in this region are likely to be generated by a thermochemical plume, which might extend from the core-mantle boundary to the base of the plate (Ni et al. 2002). Finally, sets of stepped peneplains, marked gradients in the elevation of uplifted coral reef terraces, and discrete phases of river incision, are characteristic

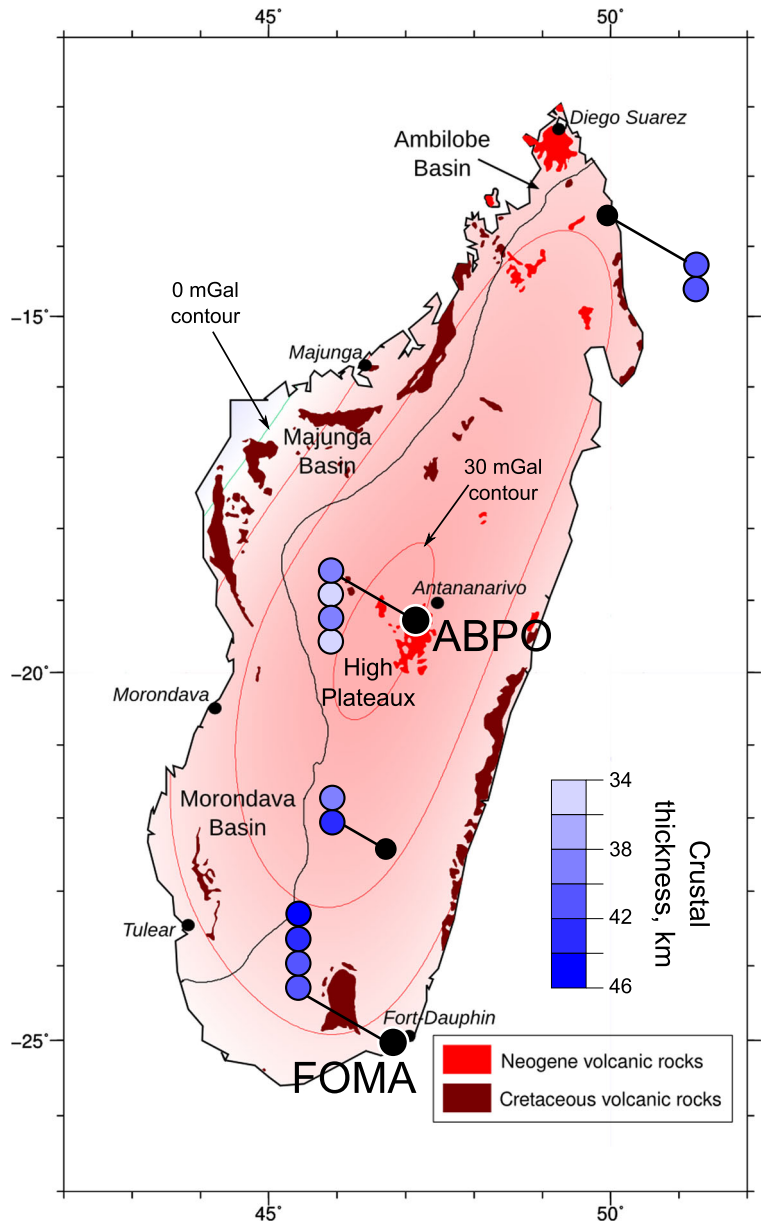

Fig. 1 Outcrops of volcanic rock and long wavelength free-air gravity anomaly centered on Madagascar (*pink shading*). Contour interval = 10 mGal; green contour = 0 mGal. The gravity field has been passed through a 30-km-wide cosine arch filter to remove wavelengths < 800 km, providing a crude proxy for mantle convection (e.g. Paul et al. 2014). Other crustal thickness data from Chaheire et al. (2010) — 21 receiver functions; Rindraharisaona et al. (2013) — 21 receiver functions and Rayleigh wave group velocities; Rambolamanana et al. (1997) — forward models of group velocities and hypocentral parameters; Pasaynos and Nyblade (2007) — fundamental mode surface waves

geomorphic signatures of a landscape responding to a mantle upwelling (e.g. De Wit, 2003; Al-Hajri et al. 2010; Roberts et al. 2012).

Fourno and Roussel (1994) and Rakotondraompiana et al. (1999) inverted gravity data to discover an elongate ∼N-S trending zone of thinned crust and asthenospheric upwelling, consistent with Neogene volcanism (Fig. 1), across the central High Plateaux. Discrete clusters of seismic activity have been used to propose a model in which Madagascar currently sits at the initial stage of E-W rifting (e.g. Bertil and Regnoult, 1998; Kusky et al. 2007, 2010). Stamps et al. (2008) describe a broad N-S deformation zone through Madagascar, similar to a diffuse plate boundary.

Knowledge of crustal structure and thickness in the center and at the coast of the island may therefore place useful constraints on sub-lithospheric mantle dynamics. Chaheire et al. (2010) inverted 21 receiver functions to calculate a consistent crustal thickness of 38–44 km beneath four seismometer stations on Madagascar. They also noted an S-wave velocity discontinuity at ∼20-km depth. More recently, Rindraharisaona et al. (2013) jointly inverted 21 receiver functions and Rayleigh wave group velocities from 4 seismic stations to obtain a similar range of crustal thicknesses: 35–42 km (see Fig. 1). Others have calculated a maximum Moho depth of ∼42 km in central Madagascar, based on simple forward models of group velocities and hypocentral parameters (Rakotondrainibe 1977; Rambolamanana et al. 1997). This depth did not vary greatly across the island. However, other studies that employ a greater range of data demonstrate a pronounced crustal thinning in the center of the island. Pasaynos and Nyblade (2007) used fundamental mode surface waves to argue for a crustal thickness of 35 km in the island's center; the CRUST 2.0 model, based on surface waves, free oscillation data, and body wave travel times, suggests values as low as 36 km (Bassin et al. 2000).

Here, a subset of receiver functions calculated from two three-component broadband seismometers is used to determine crustal structure beneath upland (station ABPO: 1528 m) and lowland (station FOMA: 28 m) regions of Madagascar. While ABPO is located on Archean basement gneisses, the rocks around FOMA are a more complicated mélange of sediments, ultramafics, and Cretaceous-aged basalt. Results are then linked to a new analysis of shear wave splitting under Madagascar, in order to assess the principal direction of mantle flow.

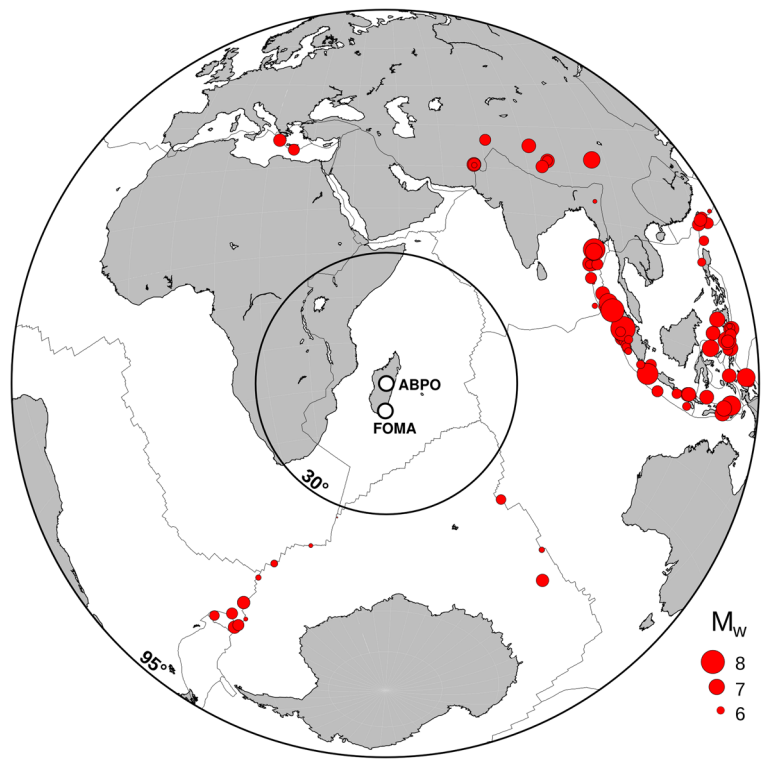

Fig. 2 Location of 128 earthquakes used in this study. *Small circles* = events recorded by stations ABPO and FOMA, scaled according to moment magnitude. *Thin lines* = plate boundaries. Seismograms were selected for deconvolution if events occurred between 30° and 95° angular distances from the seimometers

2 Receiver function analysis

The one-dimensional structure of the crust beneath a seismic station is found by exploiting earthquake records of three-component, broadband seismometers (Langston 1979). Thirty-four records were used, from the GEOSCOPE station FOMA located on the SE Malagasy coast, and a further 94 records from the IRIS station ABPO, located close to the capital Antananarivo in the central High Plateaux (Fig. 2). These databases were searched using http://ears.iris.washington.edu/ and http://geoscope.ipgp.fr/index.php/ (last accessed June 2014). Most events used in this study come from the northeast quadrant, along the Sumatra-Java-Philippine subduction zone.

The time series recorded on each component is the convolution of source mechanism and propagation effects, and instrumental response. Ground displacement, $D(t)$, for a P-wave is given by

$$D_{[Z,R,T]}(t) = S(t) * E_{[Z,R,T]}(t) * I(t), \quad (1)$$

where $S(t)$ is the source mechanism, $E(t)$ is the impulse response of Earth's structure, $I(t)$ is the instrument response, and Z, R and T are the vertical, radial and transverse components, respectively. At near vertical incidence, the vertical component will contain little energy from near-receiver P-to-SV conversions and multiples. Therefore, assuming any near-source effects (which will be common to all components) are contained in the source mechanism, the Z component can be approximated as

$$D_Z(t) \simeq S(t) * I(t), \quad (2)$$

that is, the source mechanism convolved with instrumental response. Assuming $I(t)$ is the same for each component, $E_R(t)$ can be calculated by deconvolving $I(t) * S(t)$ from $D_R(t)$. This deconvolution is equivalent to division in the frequency domain:

$$E_R(\omega) = \frac{D_R(\omega)}{I(\omega) * S(\omega)} \simeq \frac{D_R(\omega)}{D_Z(\omega)}. \quad (3)$$

Finally, $E_R(\omega)$ is transformed back to the time domain to retrieve the radial receiver function $E_R(t)$. The P-wave arrival is prominent on the vertical (Z) component; signal to noise ratio is improved by stacking many events at every station. One hundred twenty-eight receiver functions were calculated for

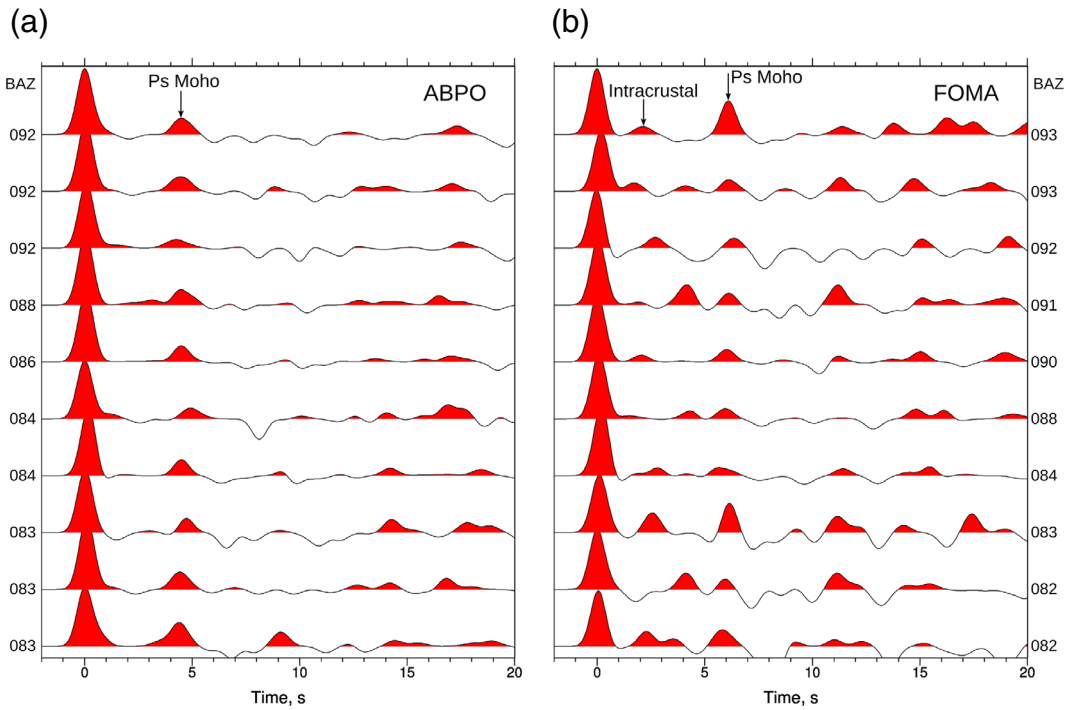

Fig. 3 Small subsets of radial receiver functions used in inverse modeling arranged by backazimuth (BAZ), quoted in degrees. **a** ABPO. Note the Ps Moho arrival around 4–5 s, and a diffuse PpPs arrival at ~14 s. **b** FOMA. Note the later, diffuse Ps arrival around 6 s, a possible intracrust velocity contrast around 2–3 s, and a highly diffuse PpPs arrival at 15–16 s

stations ABPO and FOMA using events of $M_w > 6.5$ occurring at angular distances of between 30° and 95° to Madagascar. Seismic signals will arrive at near-vertical incidence and will be sufficiently coherent for stacking. A self-consistent subset from a smaller back-azimuthal range was chosen for each station (Fig. 3).

The H-κ stacking method of Zhu and Kanamori (2000), where H refers to crustal thickness and κ is the V_p/V_s ratio, was then used to obtain cursory estimates of Moho depth (Fig. 4). This method assumes a simple, single-layered crust beneath each station, with constant P- and S-velocities. A key advantage of this grid-search technique over direct conversion from Ps arrival times to Moho depth is that data from the whole receiver function are utilized, which increases objectivity and removes the chance of misidentifying an arrival. Furthermore, it relies less upon assumptions of the crustal thickness vs. crustal velocities tradeoff, and additional a priori crustal parameters. In fact, the only a priori value used in this analysis is an average V_p for the crust. The effects of crustal velocity gradients are small.

3 Modeling of receiver functions

The crustal velocity structure is obtained through a three-stage procedure combining inversion and guided forward modeling (Davis et al. 2012). The inversion algorithm seeks to calculate the best-fitting 1D shear wave velocity structure giving rise to the receiver function at each station. Each intercrustal interface will produce peaks whose delay times depend on the velocity and thickness of layers between the interfaces. Their amplitude will depend on the velocity contrast across the interfaces. Since receiver functions are most affected by changes in V_S, V_P is kept as a constant multiple of V_S. First, the subset of receiver functions (Fig. 3) is stacked and the mean amplitude and standard deviation calculated (Fig. 5). Secondly, these receiver functions are inverted by systematically varying V_S as a function of depth for a range of V_P/V_S values. The initial velocity structure is a simple half-space model where $V_s = 4$ km s^{-1}. Our models require a minimum of a priori information, so serve as a good starting point, to be subsequently simplified in an iterative manner.

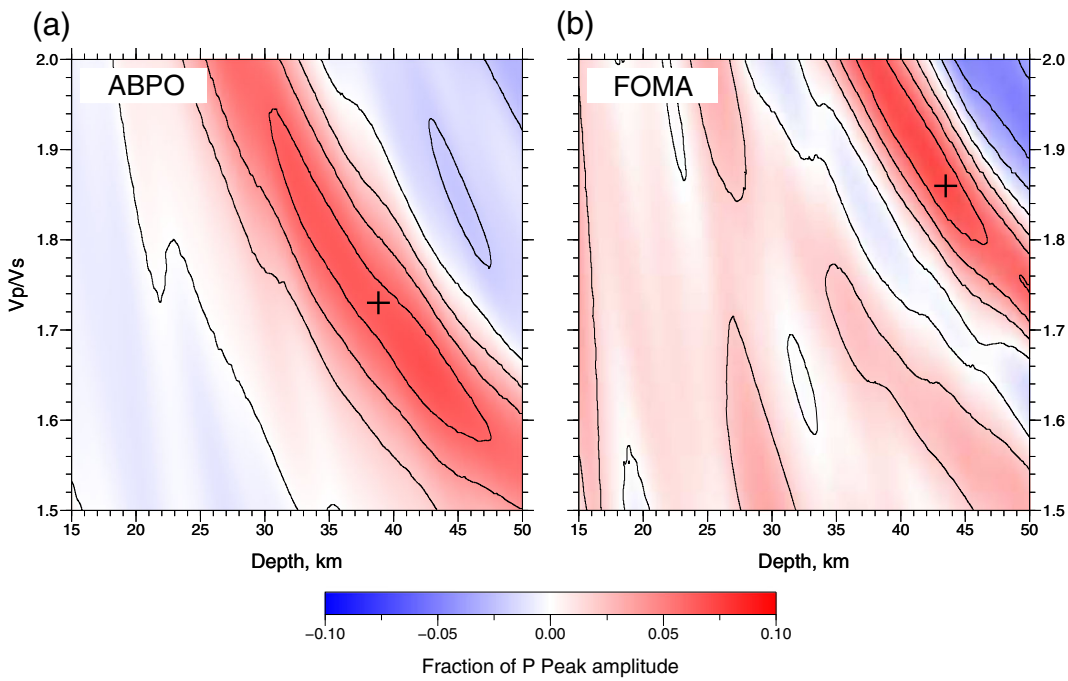

Fig. 4 H-κ stacking plots, which show how receiver function amplitude (Fig. 3) varies according to V_p/V_s ratio and Moho depth. **a** ABPO. **b** FOMA. *Thin lines* = 0.02 contours of P wave peak amplitude; *crosses* = peak stacking amplitude at optimal average crustal V_p/V_s ratio and Moho depth. Note strong trade-off between V_p/V_s ratio and Moho depth

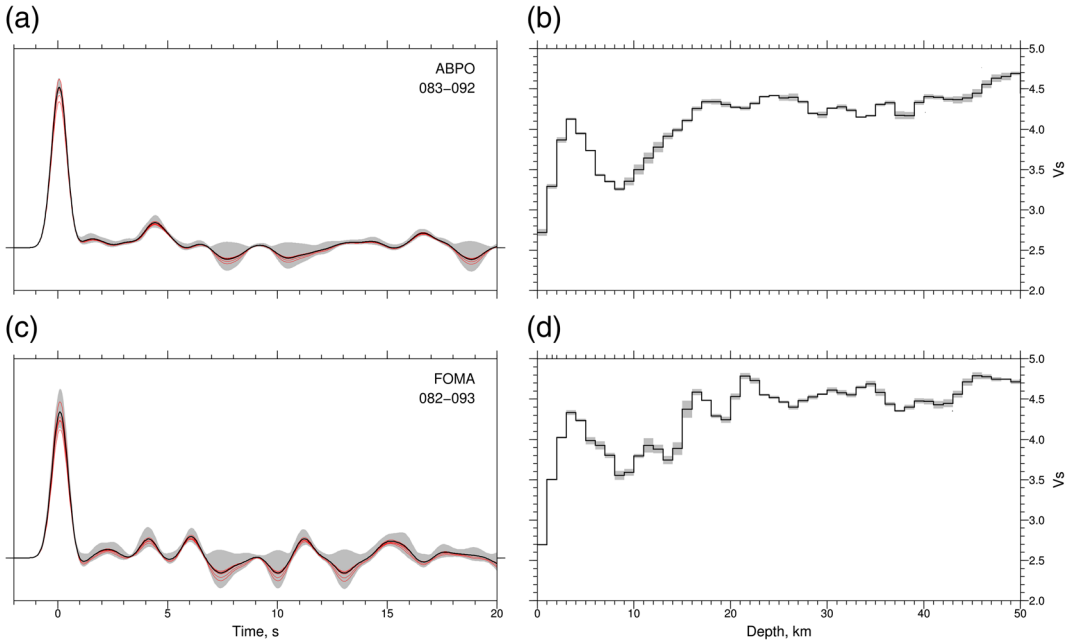

Fig. 5 Results of inverse modeling of stacked receiver functions from ABPO and FOMA. **a**, **c** *central line* with *grey* envelope = average receiver function and its standard deviation obtained by stacking many receiver functions over a small back-azimuthal range; *multiple thinner lines* = 31 best-fitting inverse models obtained using V_p / V_s values in the range 1.6–1.9 with an increment of 0.1. *Number below station* = range of backazimuths used. **b**, **d** V_s as a function of depth, retrieved by inverse modeling. *Central line* with *grey* envelope = average velocity function calculated at 1-km intervals with one standard deviation

Thirdly, a guided forward modeling approach is employed to identify the smoothest (or least complicated) velocity models that yield good fits between calculated and observed receiver functions. Layers of similar velocity in the inverse velocity model are grouped, and unnecessary depth interfaces removed. These forward models are then randomly varied to identify an optimal average model (Fig. 6). Varying the depth and magnitude of the velocity discontinuities is one method of mapping uncertainties in the stacked receiver function (e.g. the possibility of modeling intracrustal interfaces instead of the Moho) onto the solution space. This produces a range of plausible Moho depths, shown within one confidence interval (Fig. 6).

4 Shear wave splitting

Due to the tendency of olivine, the main mineral constituent of the upper mantle, to develop a lattice preferred orientation (LPO) while undergoing shear deformation, flow in the asthenosphere will manifest as seismic anisotropy. This can be illuminated by studying the shear wave splitting (SWS), and informs the pattern of mantle flow. In this technique, when an incident shear wave enters an anisotropic medium, it will become polarized into two different directions: a fast direction (ϕ) and a slow direction, which accumulate a delay time (δt) between them.

Here, we analyze shear wave splitting of teleseismic core phases (SKS and PKS) at stations ABPO and FOMA to investigate the dynamics of the upper mantle beneath Madagascar. We study M6+ events (Fig. 7) located in the epicentral distance range 88°–130° for SKS and 130°–150° for PKS, over the time range available at each station (since 2007 for ABPO, and 2008 at FOMA). All seismograms are bandpass filtered with a fixed lower cut-off at 0.04 Hz and a variable upper cut off between 0.1–0.2 Hz, to best improve the signal to noise ratio. We use SplitLab (Wüstefeld et al. 2008), a standard software package, which calculates the SWS parameters via two independent methods: rotation correlation (RC: Bowman and Ando 1987) and the tranverse energy minimization method (SC) by Silver and Chan (1988); see Fig. 8.

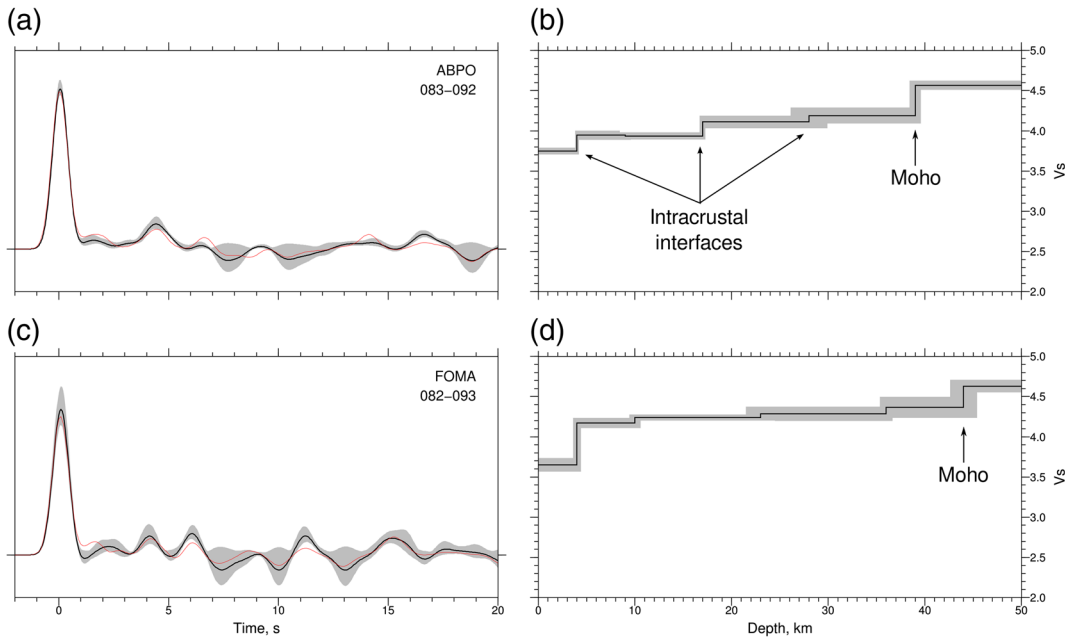

Fig. 6 Forward modeling of stacked receiver functions from ABPO and FOMA. **a**, **c** *central line* with *grey* envelope = average receiver function and its standard deviation obtained by stacking many receiver functions over a small back-azimuthal range; *thinner, lighter line* = receiver function calculated from average of the best 50 forward-modeled velocity distributions determined by randomly varying discontinuities by up to 5 km for any given velocity function. This *line* represents the ideal balance between data misfit and model roughness, i.e. the simplest model that fits the data reasonably well. *Number below station* = range of backazimuths used. **b**, **d** V_s as a function of depth, retrieved by inverse modeling. *Central line* with *grey* envelope = average velocity function and its standard deviation calculated from the best 50 models at variable (2–15 km) depth intervals. Moho at FOMA = 44 ± 1.6 km; Moho at ABPO = 39 ± 0.7 km

We visually inspect every seismogram (806 total), and all our measurements undergo strict quality control that closely follows our previous work (e.g. Eakin and Long 2013; Eakin et al. 2015). For null measurements (Fig. 8a), which designate shear waves that have not undergone splitting, our requirements are as follows: a clearly visible shear wave pulse on the radial (Q) component, high signal to noise ratio (SNR >5), low or no energy on the transverse (T) component, and initial particle motion aligned with the backazimuth. For non-null or 'split' measurements (Fig. 8b), we require a clearly defined shear wave pulse on both the radial and transverse components, initial elliptical particle motion that becomes linearized following correction, small error bars ($<$ 22.5° for ϕ, and $<$0.5 s for δt), and consistency between the RC and SC methods to within the same standard error limits. Following these criteria, we amassed 89 individual measurements at FOMA, and 82 at ABPO (Fig. 8).

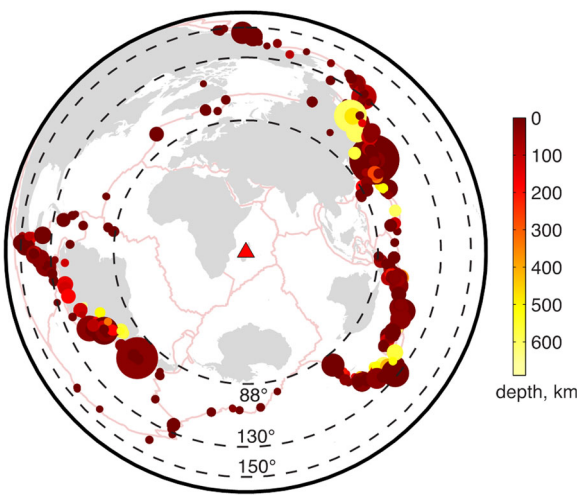

Fig. 7 Distribution of seismic events used during the SWS analysis of this study. Earthquakes are color-coded by depth and scaled in size by magnitude. There are 578 unique events plotted, most of which originate from the major subduction zones

5 Results

The seismometer station located in the central High Plateaux (ABPO) is situated 1.5 km higher than the

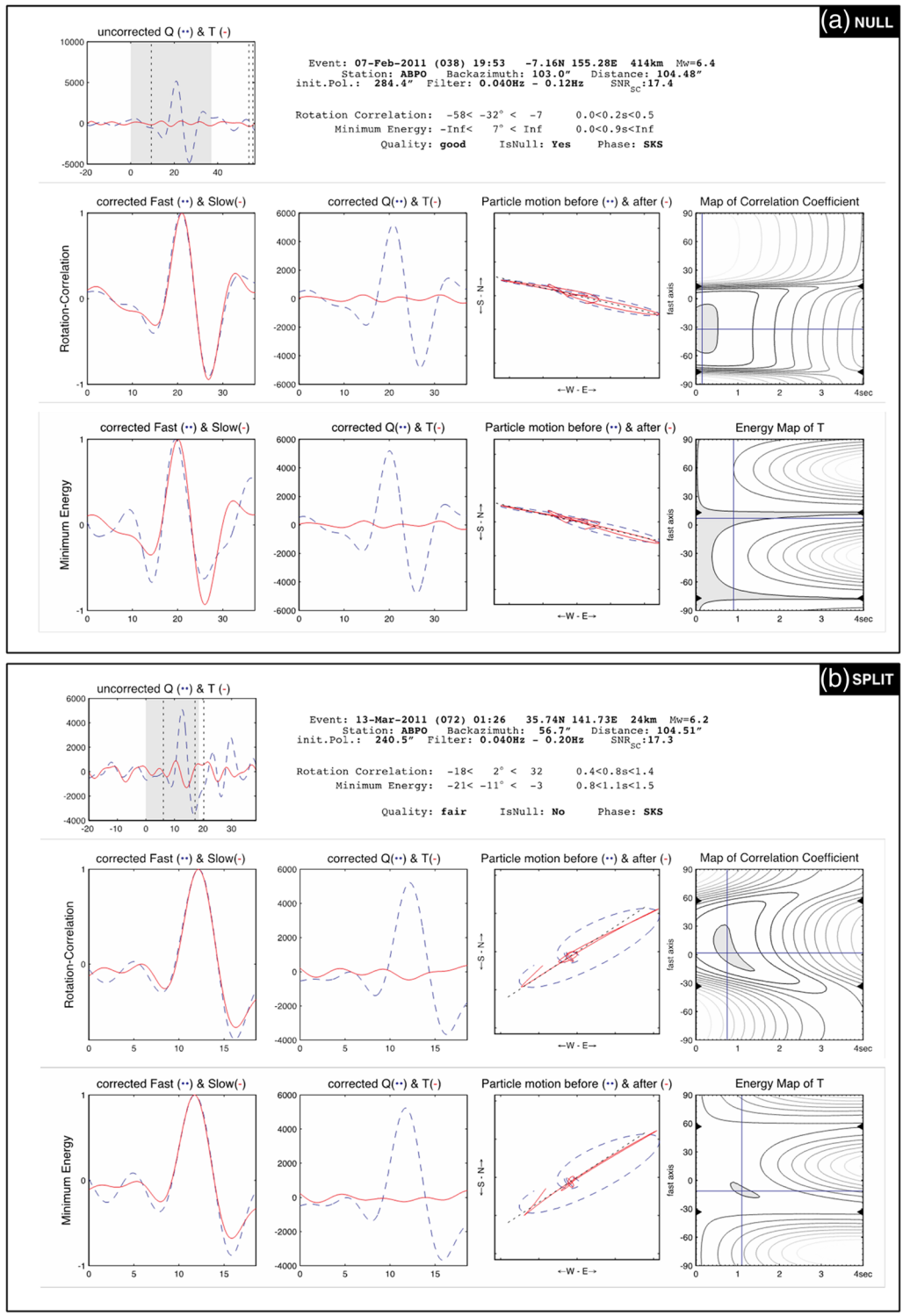

Fig. 8 Example of null (**a**) and non-null (**b**) shear wave splitting measurements at station ABPO. The diagnostic plots produced by the SplitLab program (Wüstefeld et al. 2008) are shown, with descriptions above each plot. *Q* stands for the radial component and *T* for the transverse component. The two panels correspond to the two different methods; RC on the *top* and SC on the *bottom panel*

coastal station, FOMA. The crust is 39 ± 0.7 km thick here and 44 ± 1.6 km at FOMA. At ABPO, there are more crustal discontinuities in the shear-wave velocity structure (Fig. 6b). Taking the range of possible Moho depths indicated as a grey envelope on Fig. 6, the thickest-possible crust at ABPO is ∼40 km, still 3 km thinner than the thinnest-possible scenario at FOMA. For the shear wave splitting, at both stations we recorded an overwhelming majority of null results; 99 % at FOMA (79 null SKS, 9 null PKS, 1 split SKS), and 96 % at ABPO (73 null SKS, 6 null PKS, 3 split SKS). These null measurements also originate from a wide span of backazimuths (Fig. 9) encompassing all four quadrants. As far as we are aware, these are the first shear wave splitting measurements for Madagascar, and they suggest that the upper mantle beneath the island is effectively isotropic to vertically (or close to vertical) incident *KS phases. Given the relative amplitudes of the radial and transverse components in Fig. 9, the occasional non-null measurement in our dataset is most likely related to random noise on the transverse component that has been mistakenly interpreted as a *KS pulse.

6 Discussion

The difference in crustal thickness under ABPO and FOMA cannot be explained by crustal Airy isostasy, which would necessitate a thick crustal root to support the high topography. The crustal structure beneath the center of the island, calculated by inverse and guided forward modeling of the stacked subset of receiver functions, is clearly different to that beneath the coast. Because the central Itasy and Ankaratra volcanic provinces were the focus of intense volcanic activity beginning in late Miocene times (Fig. 1), the stepped shear wave velocity structure could reflect ubiquitous igneous intrusions within the crust. This more complicated and irregular crustal V_s profile was noted by Chaheire et al. (2010), who highlighted a velocity discontinuity, almost as great as that of the Moho, at 20-km depth. Rindraharisaona et al. (2013) also noted a major 'intracrustal interface' at 18 km, approximately the same depth as the major V_s discontinuity calculated here: Fig. 6b. They then divided the crust into upper and lower portions, the boundary described by a major basaltic intrusion.

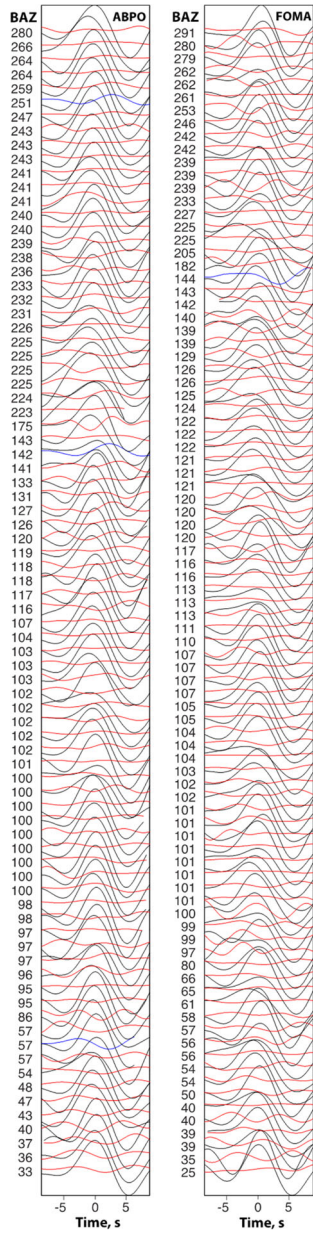

Fig. 9 Shear wave (*KS) splitting waveforms for stations ABPO and FOMA arranged by backzimuth (BAZ), quoted in degrees. The (*KS) pulse is clearly visible on the radial (*R*) component (*black lines*) for each event. Meanwhile, the transverse component (*red lines*) is relatively flat in comparison (amplitude <30 % of R), showing an absence of shear wave energy across a wide range of backazimuths. Such characteristics define null results, i.e. apparent isotropy. A small number of events (shown in *blue*) had a transverse component pattern consistent with splitting (i.e. non-null results). All the seismograms shown are scaled vertically relative to the maximum amplitude of the R component, and cross-correlated to align the main shear wave pulse of each event. Polarities have been adjusted for uniformity. A bandpass filter between 0.04–0.125 Hz has been applied

Based on uncertainties in the seismic dataset (such as the possibility of intracrustal reflections affecting our inverse models), the results demonstrate that the crust is not thick beneath highland central Madagascar, rather than it being definitely thinner than coastal areas. Our results agree with those of Pasaynos and Nyblade (2007), who also modeled crustal thinning in the central area of the island, to a minimum of 35 km (cf. Fig. 6: 39 km beneath ABPO). However, our results do not agree with those of Rindraharisaona et al. (2013), who calculated crustal thickness at FOMA to be ∼4 km greater than at FOMA. However, they ran joint inversions with Rayleigh wave group velocities, and only modeled 21 events (as opposed to >120 in this study). Moreover, these 21 events were of $M_w > 5.5$, so were more likely to include additional noise.

In terms of the SWS analysis, the abundant null measurements at both ABPO and FOMA suggest that the upper mantle beneath Madagascar is not conducive to shear wave splitting of *KS phases. The most likely explanation for this appears to be that beneath the island the upper mantle has a vertical axis of fast anisotropic symmetry, caused by vertical mantle flow (e.g. asthenospheric upwelling). Such a scenario is therefore consistent with the idea of long wavelength dynamic uplift and support for Madagascar that is required to maintain high topography over its center. Alternatively, the prevalence of nulls could also be attributed to a lack of coherent anisotropy in the upper mantle (either isotropy or strong heterogeneity).

Figure 10 is an isostatic calculation for Madagascar, where elevation is plotted as a function of lithospheric thickness and mantle density. Elevations of up to ∼2 km can be isostatically supported by a 40-km thick crust with a plate that has a thickness and mantle density of 90–160 km and 3.27–3.33 g cm^{-3} at standard temperatures and pressures (i.e. the entire range of plausible values from highly depleted to undepleted; Crosby et al. 2010), respectively.

Crustal thicknesses of under 40 km, as estimated by our receiver functions, suggest that mechanisms

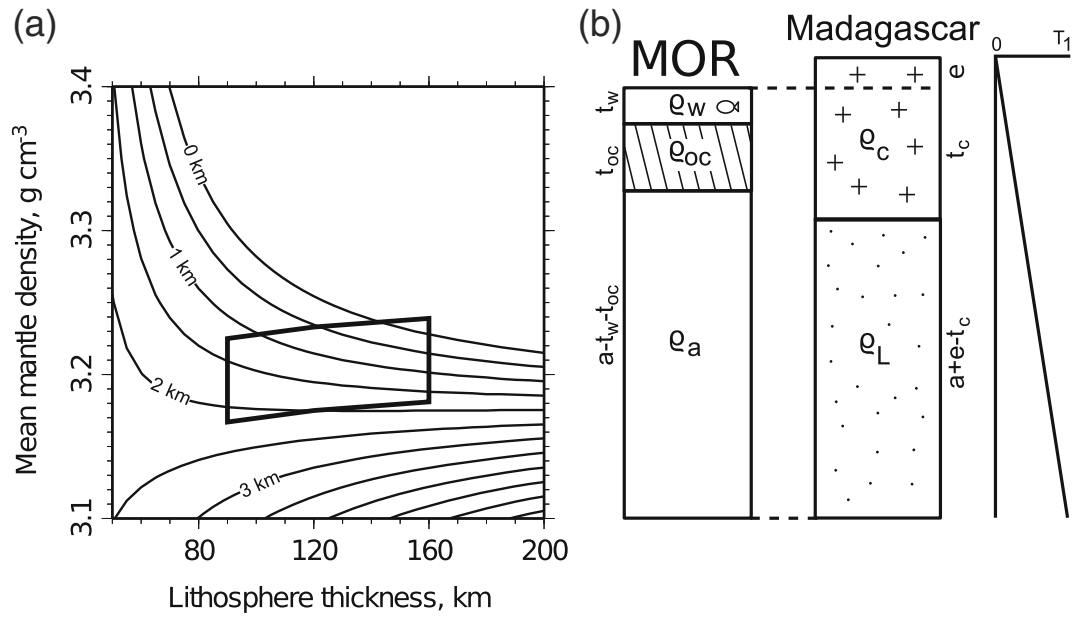

Fig. 10 Isostatic balance of Malagasy continental lithosphere against a mid-oceanic ridge (MOR) to calculate elevation (e) as a function of lithospheric thickness (a + e) and density (after Roberts et al. 2012). Density of sea-water, ρ_w = 1.03 g cm^{-3}; oceanic crust, ρ_{oc} = 2.80 g cm^{-3}; asthenosphere, ρ_a = 3.18 g cm^{-3}; continental crust, $\rho_c = \rho_{co}(1 - \alpha\overline{T}) \approx 2.80$ g cm^{-3}; lithospheric mantle, $\rho_L = \rho_{Lo}(1 - \alpha\overline{T})$. $\alpha = 3.28 \times 10^{-5}$ °C^{-1}; ρ_{co} = 2.85 g cm^{-3}; 3.20 ≤ ρ_{Lo} ≤ 3.60 g cm^{-3}. Crust is 40 km thick (Chaheire et al. 2010). **a** Contours = elevation of topography, calculated as a function of lithospheric thickness and density; interval is 0.5 km. For example, if the lithosphere (a + e) is 120 km thick, and it has an average mantle density of 3.21 g cm^{-3}, then e = 1 km. The topography of Madagascar can be reproduced for a 3.27–3.33 g cm^{-3} range of lithospheric mantle densities at standard temperature and pressure, and a 90–160-km range of lithospheric thicknesses (*black box*). **b** Cartoon showing model setup. *Left panel* = column at MOR; *central panel* = continental column; *right panel* = continental geotherm

other than isostasy (i.e. dynamic support) operate to maintain such long wavelength topography over long periods of time. Dynamic support would be consistent with the long wavelength free-air gravity anomaly centered on Madagascar, intense Neogene volcanic activity and geomorphologic evidence (such as uplifted coral reef and stepped peneplains) for rapid vertical motions and erosion rates through Neogene times (Roberts et al. 2012).

7 Conclusions

Crustal receiver functions have been modeled from two broadband seismometer stations located at the high center and southeast coast of Madagascar. The crust is ∼5 km thinner beneath the center of the island and the crustal structure more complicated: the more pronounced and frequent discontinuities in the shear-wave velocity structure could reflect well-documented local igneous intrusions. Shear wave splitting analyses at the same stations reveal robust and pervasive null measurements, suggesting a vertical axis of fas anisotropic symmetry, likely caused by vertical mantle flow beneath the island. These findings are the opposite to the situation that would be expected with Airy isostasy (i.e. highlands supported by a thick crustal root). These data, together with other geomorphic and long wavelength gravity anomaly evidence, suggest that Madagascar's topography is maintained dynamically by sub-lithospheric mantle processes, such as an upwelling in the asthenospheric mantle.

Acknowledgments This research has benefited from discussions with A. Gilligan, G. Roberts, N. White and M. Davis, and from technical support from I. Frame. JDP is supported by BP Exploration. The comments of two anonymous reviewers greatly strengthened the manuscript. Figures were prepared using Inkscape and GMT4.2.0.

References

Al-Hajri Y, White N, Fishwick S (2010) Scales of transient convective support beneath Africa. Geol 37(10):883–886

Bardintzeff J-M, Liégeois JP, Bonin B, Bellon H, Rasamimanana G (2009) Madagascar Volcanic provinces linked to the Gondwana break-up : geochemical and isotopic evidences for contrasting mantle sources. Gondwana Res 18:295–314

Bassin C, Laske G, Masters G (2000) The current limits of resolution for surface wave tomography in north america. EOS Transactions 81:F897

Bertil D, Regnoult J (1998) Seismotectonics of Madagascar. Tectonophysics 294:57–74

Bourgeat F, Petit M (1969) Contribution à l'étude des surfaces d'aplanissement sur les hautes–Terres centrales. Annales Géographiques 426:158–188

Bowman JR, Ando M (1987) Shear-wave splitting in the upper-mantle wedge above the Tonga subduction zone. Geophys J Int 88(1):25–41

Chaheire M, Chamassi M, Moussa A, Rakotondraibe T, Rakotozafy H, Rambolamanana G (2010) Modèles de vitesses des ondes s à Madagascar par application de la fonction reécepteur. MadaGéo 15:29–33

Crosby AG, Fishwick S, White N (2010) Structure and evolution of the intracratonic Congo Basin. Geochemistry Geophysics Geosystems 11:Q06010

Davis MW, White NJ, Priestley KF, Baptie BJ, Tilmann FJ (2012) Crustal structure of the British Isles and its epeirogenic consequences. Geophys J Int 190:705–725

Eakin CM, Long MD (2013) Complex anisotropy beneath the Peruvian flat slab from frequency-dependent, multiple-phase shear wave splitting analysis. J Geophys Res 118(9):4794–4813

Eakin CM, Long MD, Wagner LS, Beck SL, Tavera H (2015) Upper mantle anisotropy beneath Peru from SKS splitting: constraints on flat slab dynamics and interaction with the Nazca Ridge. Earth Planet Sci Lett 412:152–162

Fishwick S, Bastow I (2011) Towards a better understanding of African topography, a review of passive-source seismic studies of the African crust and upper mantle. In: Van hinsbergen DJJ, Buiter SJH, Torsvik TH, Gaina C, Webb SJ (eds) The formation and evolution of Africa: a synopsis of 3.8 GA of Earth history, vol 357, pp 343–371

Fourno J-P, Roussel J (1994) Imaging of the Moho depth in Madagascar through the inversion of gravity data: geodynamic implications. Terra Nova 6:512–519

Kusky T, Toraman E, Raharimahefa T (2007) The Great Rift Valley of Madagascar: an extension of the Africa–SoMali diffuse plate boundary? Gondwana Res 11:577–579

Kusky T, Toraman E, Raharimahefa T, Rasoazanamparany C (2010) Active tectonics of the alaotra–Ankay Graben System, Madagascar: possible extension of SoMalian–African diffusive plate boundary? Gondwana Res 18:274–294

Langston C (1979) Structure under Mount Rainier, Washington, inferred from teleseismic body waves. J Geophys Res 84(B9):4749–4762

Ni S, Tan E, Gurnis M, Helmberger D (2002) Sharp sides to the African superplume. Science 296:1850–1852

Panning MP, Romanowicz BA (2006) A three dimensional radially anisotropic model of shear velocity in the whole mantle. Geophys J Int 167:361–379

Pasaynos ME, Nyblade AA (2007) A top to bottom lithospheric study of Africa and Arabia. Tectonophysics 444:27–44

Paul JD, Roberts GG, White N (2014) The African landscape through space and time. Tectonics 33(6):898–935

Rakotondrainibe SA (1977) Contribution à l'étude de la sismicité de Madagascar. Thèse de Doctorat és-Sciences. Université Antananarivo, Madagascar

Rakotondraompiana S, Albouy Y, Piqué A. (1999) Lithospheric model of the Madagascar Island (western Indian Ocean): a new interpretation of the gravity data. Journal of African Earth Sciences 28:961–973

Rambolamanana G, Suhadolc P, Panza GF (1997) Simultaneous inversion of hypocentral parameters and structure velocity of the central region of Madagascar as a premise for the mitigation of seismic hazard in antananarivo. Pure Appl Geophys 149(4):707–730

Rindraharisaona EJ, Guidarellia M, Aoudiaa A, Rambolamanana G (2013) Earth structure and instrumental seismicity of Madagascar: implications on the seismotectonics. Tectonophysics 594:165–181

Roberts G, Paul J, White N, Winterbourne J (2012) Temporal and spatial evolution of dynamic support from river profiles: a framework for Madagascar. Geochemistry, Geophysics, Geosystems 13(4):040. doi:10.1029/2012GC004

Silver P, Chan W (1988) Implications for continental structure and evolution from seismic anisotropy. Nature 335:34–39

Simmons NA, Forte AM, Grand SP (2009) Joint seismic, geodynamic and mineral physical constraints on three-dimensional mantle heterogeneity: implications for the relative importance of thermal versus compositional heterogeneity. Geophys J Int 17:1284–1304

Stamps D, Calais E, Sarla E, Hartnady C, Nocquet J-M, Ebinger C, Fernandes R (2008) A kinematic model for the East African Rift. Geophysical Research Letters 35:L05,304

Wells NA, Andriamihaja B (1993) The initiation and growth of gullies in Madagascar: are humans to blame? Geomorphology 8:1–46

De Wit M (2003) Madagascar: heads it's a continent, tails it's an island. Ann Rev Earth Planet Sci 31:213–248

Wüstefeld A, Bokelmann G, Zaroli C, Barrusol G (2008) Splitlab: A shear-wave splitting environment in Matlab. Computational Geoscience 34(5):515–528

Zhu L, Kanamori H (2000) Moho depth variation in southern California from teleseismic receiver functions. J Geophys Res 105:2969–2980